

# Multimodal imaging based on MRI and PET reveals [ $^{18}\text{F}$ ]FLT PET as a specific and early indicator of treatment efficacy in a preclinical model of recurrent glioblastoma

Aurélien Corroyer-Dulmont<sup>1,2,3,4</sup> · Elodie A. Pérès<sup>1,2,3,4</sup> · Aurélie N. Gérault<sup>1,2,3,4</sup> · Ariel Savina<sup>5</sup> · Fanny Bouquet<sup>5</sup> · Didier Divoux<sup>1,2,3,4</sup> · Jérôme Toutain<sup>1,2,3,4</sup> · Méziane Ibazizène<sup>1,2,3,4</sup> · Eric T. MacKenzie<sup>1,2,3,4</sup> · Louisa Barré<sup>1,2,3,4</sup> · Myriam Bernaudin<sup>1,2,3,4</sup> · Edwige Petit<sup>1,2,3,4</sup> · Samuel Valable<sup>1,2,3,4</sup>

Received: 30 June 2015 / Accepted: 8 October 2015  
© Springer-Verlag Berlin Heidelberg 2015

## Abstract

**Purpose** The primary objective of this study was to compare the ability of PET and MRI biomarkers to predict treatment efficacy in a preclinical model of recurrent glioblastoma multiforme.

**Methods** MRI (anatomical, diffusion, vasculature and oxygenation) and PET ([ $^{18}\text{F}$ ]FDG and [ $^{18}\text{F}$ ]FLT) parameters were obtained 3 days after the end of treatment and compared with late tumour growth and survival.

**Results** Early after tumour recurrence, no effect of treatment with temozolomide combined with bevacizumab was observed on tumour volume as assessed by T2-W MRI. At later times, the treatment decreased tumour volume and increased survival. Interestingly, at the earlier time, temozolomide+bevacizumab decreased [ $^{18}\text{F}$ ]FLT uptake, cerebral blood

volume and oedema. [ $^{18}\text{F}$ ]FLT uptake, oedema and cerebral blood volume were correlated with overall survival but [ $^{18}\text{F}$ ]FLT uptake had the highest specificity and sensitivity for the early prediction of treatment efficacy.

**Conclusion** The present investigation in a preclinical model of glioblastoma recurrence underscores the importance of multimodal imaging in the assessment of oedema, tumour vascular status and cell proliferation. Finally, [ $^{18}\text{F}$ ]FLT holds the greatest promise for the early assessment of treatment efficacy. These findings may translate clinically in that individualized treatment for recurrent glioma could be prescribed for patients selected after PET/MRI examinations.

**Keywords** PET · MRI · Imaging biomarker · Glioblastoma · Recurrence · Treatment efficacy

**Electronic supplementary material** The online version of this article (doi:10.1007/s00259-015-3225-0) contains supplementary material, which is available to authorized users.

✉ Samuel Valable  
valable@cyceron.fr

<sup>1</sup> CNRS, UMR 6301 ISTCT, CERVOxy and LDM-TEP groups. GIP CYCERON, Bd H Becquerel, BP 5229, 14074 Caen Cedex, France

<sup>2</sup> CEA, DSV/I2BM, UMR 6301 ISTCT, CERVOxy and LDM-TEP groups. GIP CYCERON, Bd Henri Becquerel, BP 5229, 14074 Caen Cedex, France

<sup>3</sup> UNICAEN, UMR 6301 ISTCT, CERVOxy and LDM-TEP groups. GIP CYCERON, Bd Henri Becquerel, BP 5229, 14074 Caen Cedex, France

<sup>4</sup> Normandie Univ, Esplanade de la Paix, 14032 Caen Cedex, France

<sup>5</sup> Roche SAS, 30, cours de l'Île Seguin, 92650 Boulogne-Billancourt, France

## Introduction

Conventional treatments for glioblastoma multiforme (GBM) involve the use of alkylating chemotherapy based on temozolomide (TMZ) combined with radiotherapy [1, 2] following surgery. However, in humans recurrence is always observed (between 27 and 45 weeks after the end of first-line treatment) [3]. A salvage treatment regimen, used as second-line treatment, is consequently proposed to patients. For GBM, second-line treatment involves chemotherapy associated or not with an antiangiogenic treatment, bevacizumab [4]. Indeed, GBM is highly vascularized and the inhibition of vascular endothelial growth factor has been reported as be the most effective strategy for the treatment of GBM [5]. Although several phase II studies have shown marked responses to bevacizumab in

terms of progression-free survival in patients with recurrent GBM [6–8], its effect on overall survival is not convincing.

The difficulty in demonstrating treatment efficacy in recurrent GBM may also be due to the absence of relevant imaging biomarkers. As for first-line treatment, the early evaluation of treatment remains a critical point in considering the use of antiangiogenic treatments, and is well known to change the interpretation of conventional T1-W MRI with gadolinium chelates. Conventional MRI (T2-W and T1-W), associated or not with diffusion-weighted imaging and perfusion-weighted imaging, is the standard examination in a patient before any treatment; thereafter, tumour growth and relapse are often detected by conventional MRI alone. In contrast, better adapted imaging paradigms have proven to be powerful methodologies for early assessment of treatment efficacy [9–12]. Similarly, multimodal approaches are recognized as valuable tools for characterizing the effect of antiangiogenic treatments on the vasculature. For instance, recent developments in MRI have allowed its use in estimating the degree of hypoxia [13, 14] and the architecture of vessels in evaluating the efficacy of an antiangiogenic treatment [15].

Beyond the assessment of the vascular compartment with MRI, it is also important to characterize the behaviour of tumour cells. With respect to PET imaging, as well as the evaluation of glucose metabolism with 2-deoxy-2- $^{18}\text{F}$ fluoro-D-glucose ( $^{18}\text{F}$ FDG), other functional parameters can be analysed such as cell proliferation with 3'- $^{18}\text{F}$ fluoro-3'-deoxy-L-thymidine (FLT) [9, 16] and amino acid uptake by *o*-(2- $^{18}\text{F}$ fluoroethyl)-L-tyrosine (FET) [17] or methyl- $^{11}\text{C}$ -L-methionine (MET) [18]. These specific imaging biomarkers have proven to be remarkably robust in the early determination of therapeutic efficacy in newly diagnosed GBM [9, 11, 12, 19].

The aim of this study was to evaluate at a preclinical level the use of multimodal MRI/PET imaging in predicting and characterizing the efficacy of chemotherapy combined with an antiangiogenic treatment in recurrent GBM. To replicate the most salient aspects of GBM in the clinical setting, we used the U251 human GBM model that displays numerous human pathological characteristics (such as central necrosis, vascular heterogeneity and hypoxia [20]). To assess the efficacy of treatment, MRI and PET imaging were performed at an early time (3 days,  $t_1$ ) after the end of second-line treatment and were compared with late anatomical MRI (10 and 17 days,  $t_2$  and  $t_3$ ) and overall survival. We specifically focused on oedema volume, diffusion, perfusion index, cerebral blood volume (CBV), oxygen saturation (SatO<sub>2</sub>-MRI) and vascular permeability. For PET biomarkers, we focused on glucose metabolism and cell proliferation using  $^{18}\text{F}$ FDG and  $^{18}\text{F}$ FLT, respectively. Immunohistochemical studies with rat endothelial cell antigen (RECA-1), Ki67 and pimonidazole were performed to confirm the imaging results.

## Materials and methods

### Cell cultures, rat glioma model and treatments

Cells of the human U251 glioma cell line (National Cancer Institute) were grown in DMEM (Sigma-Aldrich, France), 1 g/l of glucose supplemented with 2 mM glutamine (Gibco, France) and 10 % fetal calf serum (Eurobio, France). The animal investigations were performed in compliance with the current European directive (2010/63/EU) in authorized housing and laboratories (B14118001) and with the permission of the regional committee on animal ethics (CENOMEXA, 0611-02). The rats were kept in specific pathogen-free housing and were fed  $\gamma$ -irradiated laboratory food and water ad libitum. Rats were manipulated under deep anaesthesia (5 % isoflurane for induction, 2 % for maintenance, in 70 % nitrous oxide/30 % oxygen). Body temperature was monitored and maintained at  $37.5 \pm 0.5$  °C throughout the experiments.

Nude athymic rats (200 – 250 g, three months old, male, Central Animal Care Facility of the University of Caen, France) were placed in a stereotactic head holder and a scalp incision was performed along the sagittal suture. A burr hole of diameter 1 mm was drilled in the skull, 3 mm lateral to the bregma. U251 cells ( $5 \times 10^4$  cells in 3  $\mu\text{l}$  PBS containing glutamine 2 mM) were injected over 6 min via a fine needle (30G) connected to a Hamilton syringe [21]. The injection site was the right caudate putamen at a depth of 6 mm. Eight animals per group were allocated for all imaging studies (except for  $^{18}\text{F}$ FLT PET with four animals per group) following a calculation of sample size; three additional rats were autopsied at the time of the last PET session for histological analysis. The number of rats studied was 49. TMZ (10 mg/kg in saline, dose chosen to enable tumour recurrence) was administered alone to all animals by gavage daily for 5 days after initial tumour growth. Recurrence was then confirmed by MRI (about 4 weeks later). To determine the added value of using bevacizumab as a second-line treatment, bevacizumab (Avastin®, Roche) was administered intraperitoneally (10 mg/kg in saline) daily for 5 days with or without TMZ at the same dose. Control animals received physiological saline both intraperitoneally and by gavage. The detailed schedule of the treatments and imaging is illustrated in Fig. 1.

### Magnetic resonance imaging

For all imaging experiments, the rat was placed in the prone position. Respiration was monitored with a pressure-sensitive balloon around the abdomen. MRI was performed on a 7-T magnet (PharmaScan®; Bruker, Ettlingen, Germany). A cross coil configuration was used (volume/surface coil; Bruker). After a scout imaging scan, tumour-associated oedema was detected with a T2-W sequence (RARE, acceleration factor

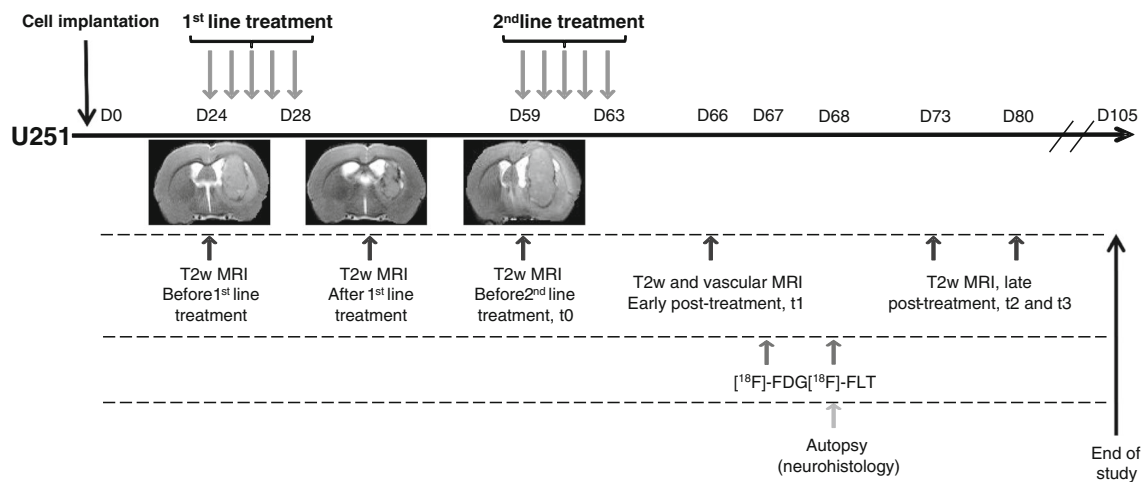


**Fig. 1** Experimental paradigm and schema for the human U251 glioma model in conjunction with MRI and PET

8; TR/TE<sub>eff</sub> 5,000/62.5 ms; number of experiments (NEX), 1; 20 contiguous slices; resolution 0.15×0.15×0.75 mm; acquisition time 2 min). Then diffusion, perfusion, saturation and vascular permeability were assessed with echo planar imaging (EPI). All EPI images were acquired with a single shot, motion artefact and ghost free, double sampling k-space coverage with identical bandwidth and geometry (ten contiguous slices, resolution 0.3×0.3×1.5 mm, except T2\*-W images which were acquired with a slice thickness of 0.3 mm for further correction of field inhomogeneities for the SatO<sub>2</sub>-MRI maps) with saturation slices at the edges of the field of view. The apparent diffusion coefficient (ADC) of water was computed from diffusion-weighted spin-echo EPI images (30 diffusion directions; TR/TE 3,000/46.3 ms; NEX 1, acquisition time 3 min 30 s) with b=1,000 s/mm<sup>2</sup> and five reference images (b≈0 s/mm<sup>2</sup>).

Vascular parameters were measured 3 days after the end of the second treatment (see Fig. 1). Prior to injection of contrast agents, five T2\*-W (TR/TE 20,000/12 ms; NEX 3, 50 contiguous slices, resolution 0.3×0.3×0.3 mm) and four T2-W (TR/TE 20,000/40 ms; NEX 3) EPI images were acquired with various echo times (TE for T2\*=12, 15, 18, 21 and 24 ms and for T2=40, 60, 80 and 100 ms).

#### *Perfusion with dynamic susceptibility contrast MRI*

Gradient-echo EPI images were then acquired for 15 s before and 105 s after a bolus injection of iron oxide particles (66 μmol/kg, P904®; Guerbet, France) [22] (TR/TE<sub>eff</sub> 400/9.17 ms; number of repetitions 300; ten slices; acquisition time 2 min).

#### *Vessel architecture with fractional CBV, vessel size index and microvessel density*

Immediately after the dynamic susceptibility contrast MRI acquisition, P904 was administered again to achieve a total

dose of 200 μmol/kg and T2\*-W (TE 12 ms) images were acquired.

#### *Vessel permeability with dynamic contrast-enhanced MRI*

Flow-sensitive alternating inversion recovery EPI images were acquired to compute T1 maps for 1 min before and 6 min after injection of Gd-DOTA (200 μmol/kg, Dotarem®; Guerbet, France) (TR/TE 10,000/7.443 ms; 15 inversion times ranging from 37.8 to 4,937.8 ms; number of repetitions 42; 1 slice; acquisition time 7 min).

#### **Positron emission tomography**

[<sup>18</sup>F]FDG was produced by Cyclopharma (France). [<sup>18</sup>F]FLT was provided by the LDM-TEP group (UMR 6301 ISTCT). Images were acquired using an Siemens Inveon® preclinical PET system on two consecutive days (see Fig. 1). An 20-min X-ray scan was employed to generate attenuation maps just prior to an emission scan initiated 60 min ([<sup>18</sup>F]FDG) or 40 min ([<sup>18</sup>F]FLT) after radiotracer injection (66 MBq/kg [<sup>18</sup>F]FDG, 66 MBq/kg [<sup>18</sup>F]FLT) into the caudal vein. All images were reconstructed using the iterative OSEM-2D algorithm.

#### **Image processing and analysis**

Image analysis was performed with in-house macros based on the ImageJ software (<http://rsb.info.nih.gov/ij/>, 1997 – 2014). PET data were analysed using PMOD 3.1 [23].

#### *MRI tumour volume*

Tumours were delineated manually on all adjacent T2-W slices. Tumour volume was calculated by multiplication of the sum of contiguous tumour surface areas by the slice

thickness. The region of interest (ROI) corresponding to the tumour, or to the mirror ROI in the healthy contralateral side, was then used for all other parameters.

#### *Vascular parameters*

Relative cerebral blood flow (CBF) maps as an index of perfusion were obtained from the first pass of P904. Fractional CBV (fCBV) maps (expressed as a percentages), vessel size index (VSI) maps (expressed in micrometres) and microvessel density (MVD) maps (expressed in arbitrary units) were calculated according to previously published methods [9, 24]. Permeability was studied on volume transfer coefficient ( $K^{\text{trans}}$ ) maps computed from dynamic T1 maps during the injection of Gd-DOTA. SatO<sub>2</sub>-MRI maps were computed from the equation described by Lemasson et al. [13]. Briefly, SatO<sub>2</sub>-MRI maps were calculated as a function of the T2\* signal after correction for inhomogeneities, blood volume and T2 effects.

#### *MRI/PET coregistration*

All MRI scans were executed such that the various MRI parameters were anatomically registered to each other. A first automatic registration (PMOD 3.1) was performed between T2-W MRI (reference) and the X-ray scan (input) by normalized mutual information. When necessary, the registration was manually refined. In a second step, the PET parameters were coregistered to the MRI parameters.

#### *PET analysis*

ROIs defined on T2-W MRI images were transferred onto all PET images. To quantify [<sup>18</sup>F]FDG and [<sup>18</sup>F]FLT uptake, the measured tissue activity concentration (counts, kilobecquerels per millilitre) was divided by the injected activity in kilobecquerels per gram of body weight to give a standardized uptake value (SUV, grams per millilitre).

#### **Statistical analysis**

All data are presented as means±SD unless otherwise stated. One-way ANOVA followed by Tukey's post-hoc test were used to compare differences between groups. Two-way ANOVA (group and time effects) followed by Tukey's post-hoc test were used to assess tumour volume differences between groups. A log-rank test was used to compare Kaplan-Meier curves. Statistical analyses were performed with JMP® software (SAS Institute Inc, USA).

#### **Immunohistochemistry**

Following the last PET session, each rat's brain was removed, immediately snap-frozen and stored at −80 °C. Coronal sections (30 µm) were cut on a cryostat (Leica, Germany). Immunohistochemical staining for RECA-1 (0.4 µg/ml, Abcam, France) was used to characterize glioma vascularization, for Ki67 (0.35 µg/ml, MIB-1; Dako, France) to characterize proliferation, and for pimonidazole (Hypoxyprobe®, 80 mg/kg intraperitoneally 120 min before the animal was killed; Hypoxyprobe, Burlington, MA) to characterize hypoxia. After blocking the nonspecific binding sites with bovine serum albumin 3 %/PBS/Tween 0.1 %/Triton 0.5 % for 90 min at room temperature, slices were incubated overnight with primary antibodies at 4 °C in bovine serum albumin 1 %/PBS/Tween 0.1 %/Triton 0.5 %, and the staining was revealed by a Cy3-linked goat anti-mouse IgG (1 µg/ml; Jackson ImmunoResearch, West Grove, PA). Nuclei were counterstained with Hoechst 33342 (Sigma-Aldrich). Tissue sections were examined at ×20 magnification for RECA-1, ×40 for Ki67 and ×4 for pimonidazole with a Leica DM6000 microscope in the non-necrotic core of the tumour. The tumour tissue was delimited by Hoechst 33342 counterstaining. The pimonidazole stained images of the entire tumour were quantified with the MosaicJ plugin of ImageJ. For quantification of Ki67, three slices per rat were used and nuclei were counted automatically (ImageJ) [21].

#### **Survival study**

After imaging, the rats (except those animals killed for immunohistochemistry) were followed for survival. Prior to the initiation of the study, 105 days was defined as an arbitrary endpoint for overall survival outcome. Receiver operating characteristic (ROC) thresholds were calculated for these three modalities based on a predefined survival threshold (animals killed 40 days after the end of treatment).

## **Results**

### **Effects of treatment on tumour volume and overall survival**

#### *Tumour volume and overall survival*

T2-W images were acquired 3 days after the end of the treatment (t1). In this model of recurrent GBM, delineation of the tumour volume was similar in each of the four groups at this time. An increase in the tumour

volume was observed at the late times ( $t_2$  and  $t_3$ ) in all groups except for the TMZ + bevacizumab group (Fig. 2a, b). The effect of the combined treatment

TMZ+bevacizumab was also shown by a significant increase in overall survival as compared to the other groups (Fig. 2c).

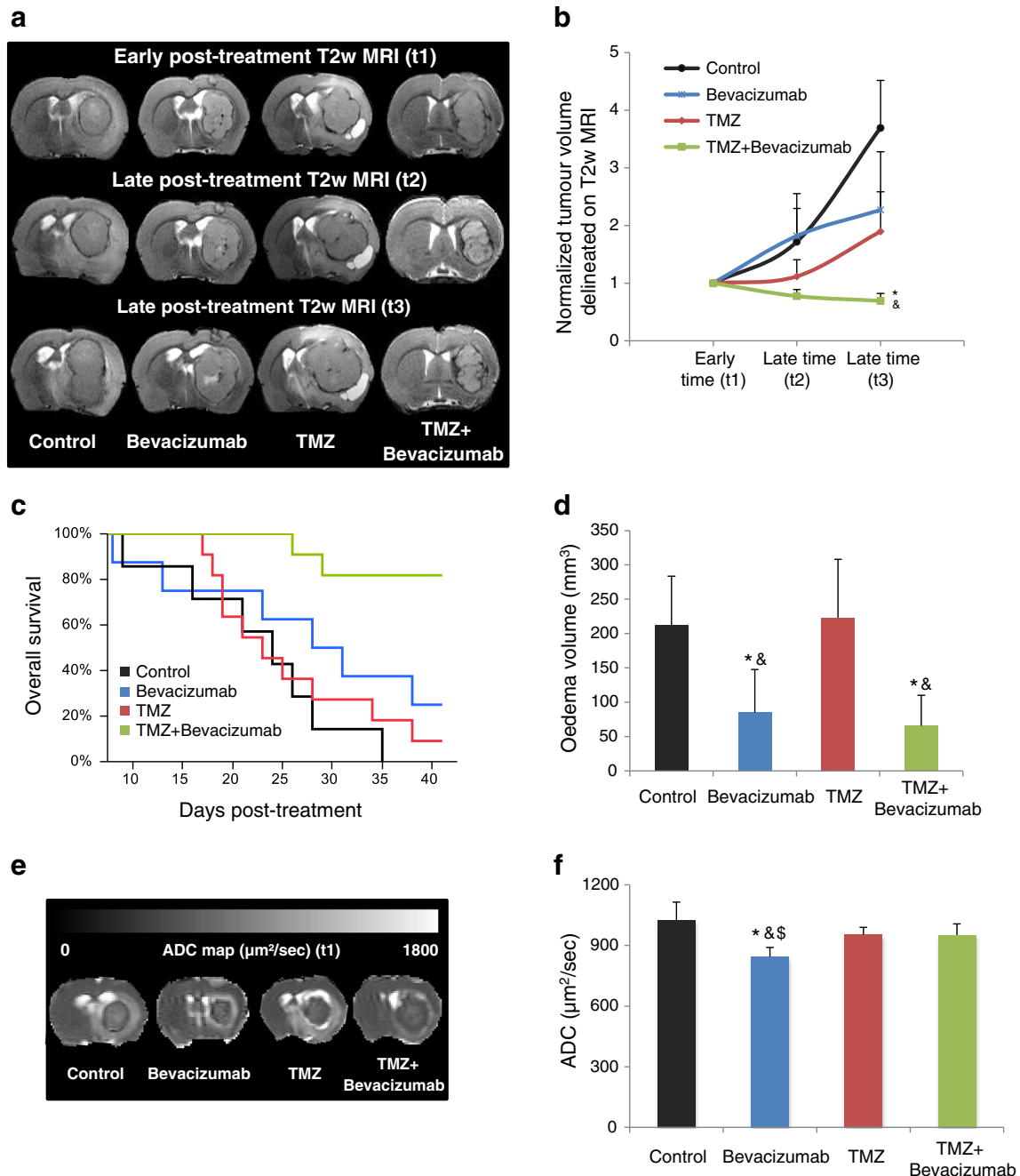


**Fig. 2** Effects of treatment on tumour volume, survival, oedema volume and diffusion of water molecules. **a** Representative T2-W MRI images for the four groups of rats early (3 days,  $t_1$ ) and late (10 days,  $t_2$ , and 17 days,  $t_3$ ) after the end of treatment. **b** Tumour volume at  $t_1$ ,  $t_2$  and  $t_3$ . The data points are means  $\pm$  SD,  $n=7$  for the control group,  $n=8$  for the bevacizumab group, and  $n=11$  for the TMZ and TMZ+bevacizumab groups at  $t_1$  ( $p<0.001$  for time effect,  $*p<0.01$  vs. the control group, and  $^{\&}p<0.01$  vs. the TMZ group). **c** Kaplan-Meier curves of survival,  $n=7$  for the control group,  $n=8$  for the bevacizumab group, and  $n=11$  for the TMZ and TMZ+bevacizumab groups ( $p<0.001$  vs. the control group

and TMZ group, and  $p<0.05$  vs. the bevacizumab group). **d** Oedematous volume at  $t_1$ . The bars are means  $\pm$  SD,  $n=8$  for the control group,  $n=7$  for the bevacizumab group, and  $n=6$  for the TMZ and TMZ+ bevacizumab groups ( $*p<0.01$  and  $p<0.001$  vs. the control group and the TMZ+ bevacizumab groups, respectively, and  $^{\&}p<0.001$  vs. the TMZ group). **e** Representative ADC maps. **f** ADC at  $t_1$ . The bars are means  $\pm$  SD,  $n=8$  for the control group,  $n=7$  for the bevacizumab group, and  $n=6$  for the TMZ and TMZ+bevacizumab groups ( $*p<0.001$  vs. the control group,  $^{\&}p<0.01$  vs. the TMZ group, and  $^{\$}p<0.01$  vs. the TMZ+bevacizumab group)



### Oedema volume

A principal feature of the U251 model is the presence of a peritumoral oedema [20]. At the early time ( $t_1$ ) and as observed in patients [25–27], bevacizumab treatment (alone or with TMZ) significantly decreased the volume of oedematous tissue (Fig. 2a, d).

### Diffusion of water molecules

In the ADC maps (Fig. 2e), a significant decrease in the ADC values in the tumour was observed but only in the bevacizumab group (Fig. 2f).

### Early MRI assessment of treatment effects on the vascular compartment

#### Perfusion

To evaluate the effects of the various treatments on perfusion, the T2\* signal during the first pass of the contrast agent (P904) was determined to compute CBF maps as an index of perfusion. CBF was significantly ( $p < 0.01$ ) higher in the TMZ group than in the bevacizumab and TMZ+bevacizumab groups (data not shown).

#### Vessel architecture (CBV, VSI, MVD)

As expected, fCBV was higher in the control and TMZ groups than in the bevacizumab and TMZ+bevacizumab groups in which the fCBV was near to that in healthy contralateral tissue (Fig. 3a, b).

VSI was not affected by treatment and relative MVD was significantly lower in the TMZ+bevacizumab group than in the TMZ group (Table 1).

#### Vascular permeability

As expected, tumour vessels showed greater permeability (expressed here as  $K^{\text{trans}}$ ) than vessels in healthy tissue (Fig. 3c). Quantitatively, only the TMZ group showed significantly higher  $K^{\text{trans}}$  values than all the other groups (Fig. 3d).

#### Oxygenation

We then sought to determine whether the changes observed in vascularization were associated with changes in oxygenation using the SatO<sub>2</sub>-MRI method. In tumours of the control group, a decrease in SatO<sub>2</sub>-MRI signal was observed in the core of the tumour with an increase in the tumour margin (Fig. 3e). In tumours of the bevacizumab group, SatO<sub>2</sub> was lower than in those of the control and TMZ groups (Fig. 3f) but was not significantly different in the TMZ+bevacizumab group.

### Immunohistochemistry

In Fig. 4a, the morphology of the cerebral vessels in animals receiving the antiangiogenic treatment was similar to that of the vessels in healthy contralateral brain. Vessels appeared to be abnormal in the TMZ group, which could explain the increase in vascular permeability (Fig. 3c, d). Quantitatively, the vascular diameter was smaller in the TMZ+bevacizumab group than in the other groups (see Table 1). This was associated with a significant decrease in the vessel number in this group (see Table 1) and resulted in a significant increase in the domains for this group (see Table 1). Pimonidazole immunostaining was also used to confirm the SatO<sub>2</sub>-MRI results. Pimonidazole staining was apparent only in the tumour of the bevacizumab group, confirming the SatO<sub>2</sub>-MRI results (Fig. 4b).

### Early PET assessment of treatment effects on the cellular compartment

To assess the effects of treatment on tumour cells, glucose consumption was measured in terms of [<sup>18</sup>F]FDG uptake. No effects of the treatments were detected (Fig. 5a, b). In contrast, lower [<sup>18</sup>F]FLT uptake was observed in the TMZ+bevacizumab group than in the control and TMZ groups (Fig. 5c, d). The decrease in tumour cell proliferation in the TMZ+bevacizumab group was also confirmed with Ki67 immunostaining (Fig. 4c). The number of Ki67-positive cells was lower in the TMZ+bevacizumab group than in the other groups and, furthermore, a slightly lower number was found in the bevacizumab group (also suggested by the [<sup>18</sup>F]FLT PET values). The numbers of Ki67-positive cells (expressed as cells per square millimetre) were: 318±48 in the control group; 193±50 in the bevacizumab group, 291±37 in the TMZ group, and 91±35 in the TMZ+bevacizumab group ( $p < 0.05$  for the bevacizumab group vs. the control group,  $p < 0.01$  for the TMZ+bevacizumab group vs. the control group, and  $p < 0.001$  for the TMZ+bevacizumab group vs. the TMZ group). Cellular swelling was observed in the TMZ and TMZ+bevacizumab groups (Fig. 4c).

### Predictive value of imaging biomarkers

Unsurprisingly, the absolute volume of tumour calculated from the late times on T2-W MRI was highly and positively correlated with overall survival. To determine the value of imaging in predicting the effect of treatment at an early phase of the disease process, we determined the degree of correlation between the different imaging biomarkers at the early time ( $t_1$ ) and overall survival. As shown in Fig. 6a, there was a linear correlation between [<sup>18</sup>F]FLT uptake and overall survival. At  $t_1$ , oedema volume and fCBV were also closely correlated with overall survival. The value of [<sup>18</sup>F]FLT uptake in

**Fig. 3** Early MRI assessment of the effects of treatment on the vascular compartment. **a** Representative fractional cerebral blood volume (fCBV) maps. **b** Relative CBV analysis (tumour compared to contralateral, mirror tissue) at  $t_1$ . The bars are means  $\pm$  SD,  $n=8$  for the control group,  $n=7$  for the bevacizumab group, and  $n=6$  for the TMZ and TMZ+ bevacizumab groups ( $*p<0.01$  vs. the control group, and  $^{\&}p<0.001$  vs. the TMZ group). **c** Representative  $K^{trans}$  maps. **d** Quantitative  $K^{trans}$  analysis at  $t_1$ . The bars are means  $\pm$  SD,  $n=8$  for the control group,  $n=7$  for the bevacizumab group, and  $n=5$  for the TMZ and TMZ+ bevacizumab groups ( $*p<0.001$  vs. the control group,  $^{\#}p<0.001$  vs. the bevacizumab group, and  $^{\$}p<0.001$  vs. the TMZ+ bevacizumab group). **e** Representative oxygen saturation maps. **f** Quantitative oxygen saturation analysis at  $t_1$ . The bars are means  $\pm$  SD,  $n=7$  for the control group,  $n=6$  for the bevacizumab group,  $n=8$  for the TMZ group, and  $n=7$  for the TMZ+bevacizumab group ( $*p<0.05$  vs. the control group, and  $^{\&}p<0.05$  vs. the TMZ group; dashed line contralateral, mirror value)

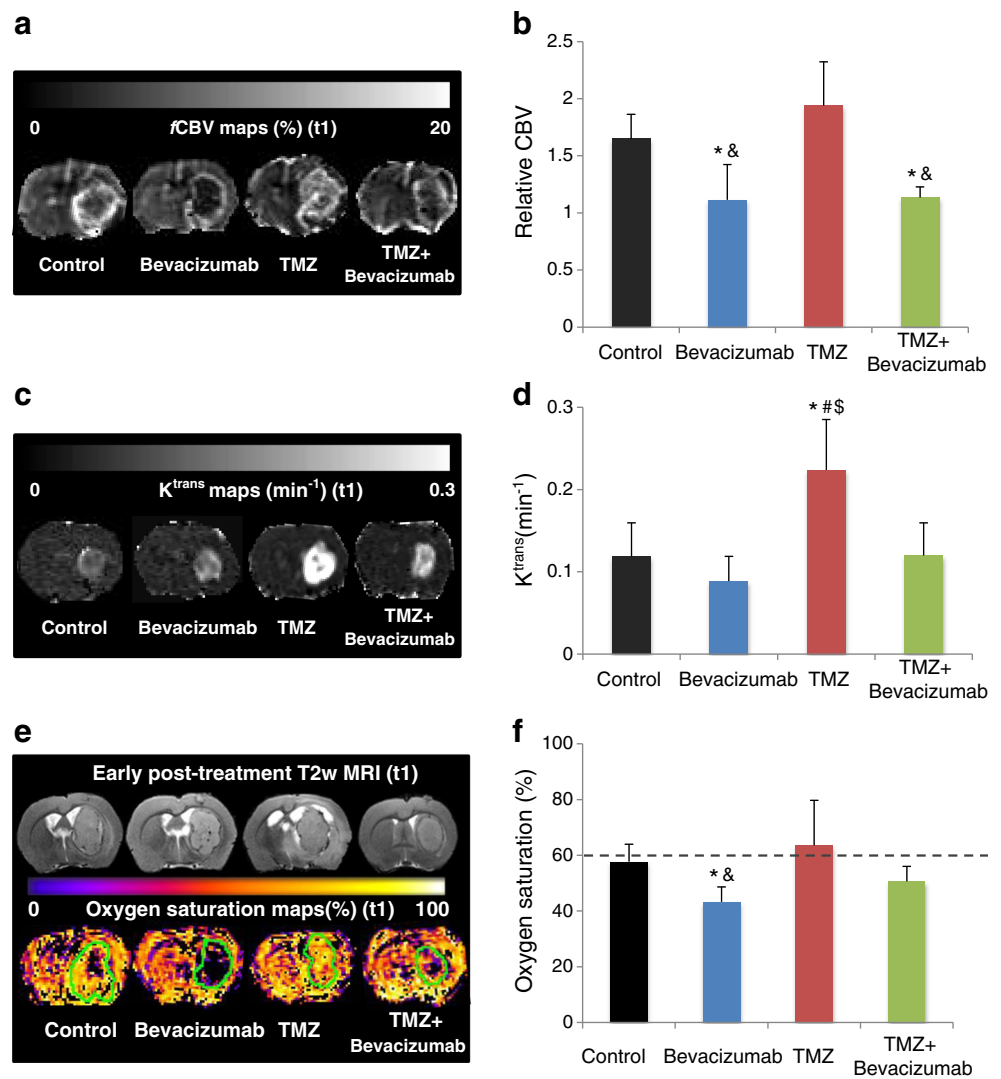


**Table 1** Effects of treatment in the vascular compartment

Vascular parameter	Group			
	Control	bevacizumab	TMZ	TMZ + bevacizumab
<b>MRI</b>				
Relative vessel size index	3.12 (0.45)	2.76 (0.40)	3.27 (0.66)	3.06 (0.38)
Relative microvascular density	0.25 (0.06)	0.24 (0.08)	0.30 (0.05)	0.21 (0.04) <sup>a</sup>
<b>Histology</b>				
Vessel diameter (μm)	4.54 (0.55)	4.46 (0.09)	4.60 (0.38)	3.45 (0.22) <sup>b</sup>
Vessel surface (%)	2.18 (0.64)	2.14 (0.82)	3.40 (1.90)	1.20 (0.45) <sup>c</sup>
Domains (μm)	34.5 (5.79)	28.6 (9.40)	24.0 (7.30)	46.1 (16.1) <sup>d</sup>

The data presented are means (SD)

<sup>a</sup> $p<0.05$  vs. TMZ group

<sup>b</sup> $p<0.05$  vs. control group, bevacizumab group and TMZ group

<sup>c</sup> $p<0.01$  vs. TMZ group

<sup>d</sup> $p<0.01$  vs. bevacizumab group and TMZ group

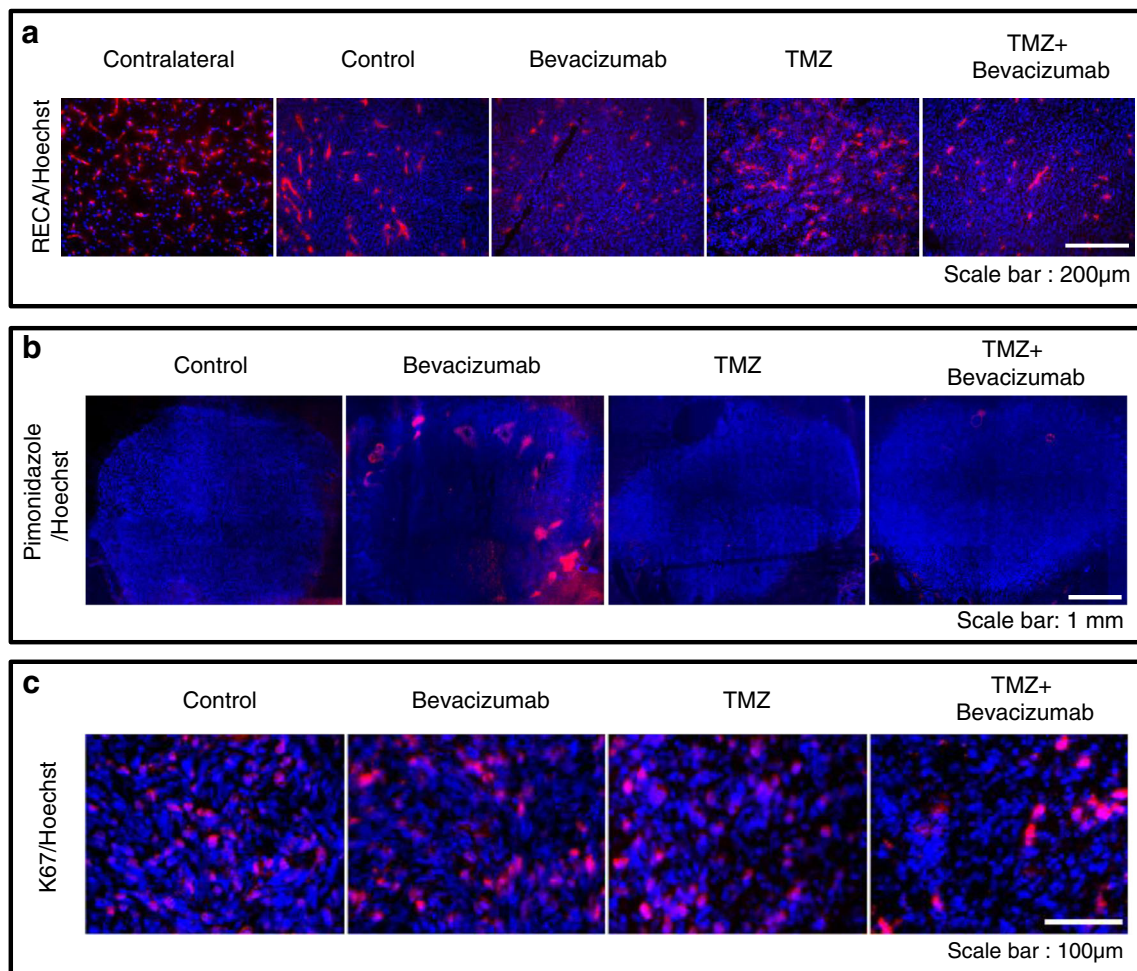


**Fig. 4** Early immunohistochemical determination of the effects of treatment on tumour vasculature, blood oxygen saturation and cell proliferation. **a** Representative images of RECA-1 immunostaining (endothelium, red) with Hoechst 33342 nuclear counterstaining (blue).

**b** Representative images of pimonidazole immunostaining (hypoxia, red) with Hoechst 33342 counterstaining (blue). **c** Representative images of Ki67 immunostaining (cell proliferation, red) with Hoechst 33342 counterstaining (blue)

predicting overall survival is demonstrated in Fig. 6b in which PET and MRI imaging in two representative animals receiving TMZ alone and TMZ in conjunction with bevacizumab is shown. ROC thresholds for the three functional modalities allowed discrimination between two populations (Fig. 6d, f, h). The specificity and sensitivity of the biomarkers were calculated, and oedema volume and fCBV were found to be associated with a certain number of false-negatives (Fig. 6c, e). Indeed, the TMZ+bevacizumab group showed a decrease in oedema volume and fCBV with a positive effect on overall survival. Of the various biomarkers, [ $^{18}\text{F}$ ]FLT showed the strongest correlation with overall survival with the highest sensitivity and specificity (Fig. 6g).

## Discussion

A trial with the aim of validating the use of bevacizumab as a second-line treatment in association with chemotherapy in the

management of recurrent GBM is underway [4, 7]. Unfortunately, most preclinical studies in the development and/or validation of innovative treatments rarely take into account inevitable recurrence. To get as close as possible to the clinical situation, we used a rat model of tumour recurrence. In this study, we were able to analyse the effect of bevacizumab associated or not with chemotherapy and to determine the predictive value of several MRI and PET biomarkers.

Using this recurrent GBM model, we found that neither TMZ nor bevacizumab alone affects tumour volume and overall survival. The low efficacy of TMZ could be due to the fact that TMZ mainly targets the tumour cells and not the vasculature and the microenvironment that are known to play key roles in tumour aggressiveness [28]. As hypothesized, bevacizumab led to an important decrease in fCBV and in oedema volume. These results concur with those observed in patients and indicate that the evaluation of oedema could be a potential biomarker to assess the efficacy of bevacizumab [10]. However, in the present investigation, we also



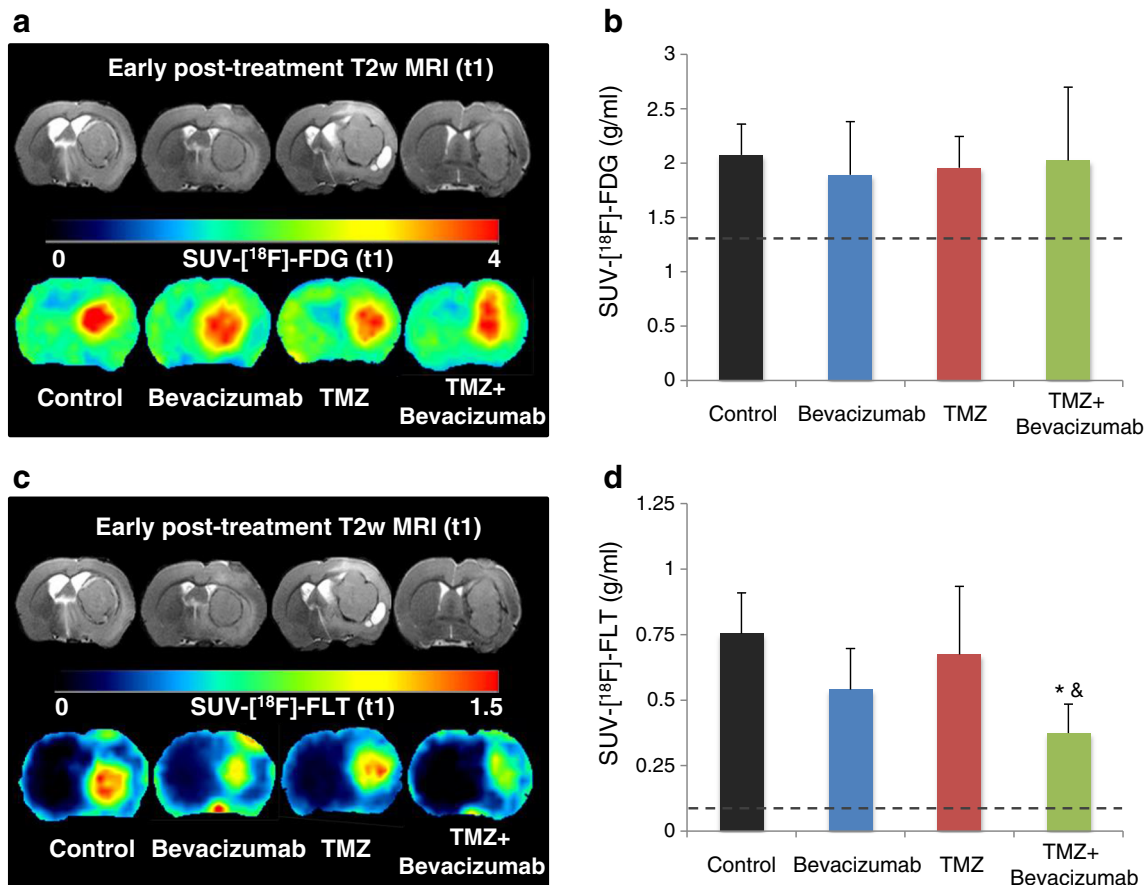


**Fig. 5** Early PET assessment of the effects of treatment on the cellular compartment. **a** Representative [<sup>18</sup>F]FDG SUV maps acquired from 60 min after injection over 20 min. **b** Quantitative [<sup>18</sup>F]FDG SUV analysis at t1. The bars are means±SD, *n*=7 for the control group, *n*=5 for the bevacizumab and TMZ groups, and *n*=6 for the TMZ+bevacizumab group (dashed line contralateral, mirror value). **c**

Representative [<sup>18</sup>F]FLT SUV maps acquired 40 min after injection over 20 min. **d** Quantitative [<sup>18</sup>F]FLT SUV analysis at t1. The bars are means±SD, *n*=5 for the control group, *n*=4 for the bevacizumab group, *n*=6 for the TMZ group, and *n*=7 for the TMZ+bevacizumab group (\**p*<0.001 vs. the control group, and &*p*<0.05 vs. the TMZ group; dashed line contralateral, mirror tissue)

demonstrated that both oedema and fCBV lack specificity since overall survival was not affected by bevacizumab alone. From a mechanistic point of view, knowing that the combination treatment controls tumour growth, we then attempted to elucidate why the combination treatment was more effective in this model of recurrent glioma. Zhou and Gallo found, in a preclinical study, that another antiangiogenic therapy (sunitinib) could increase the intratumoral concentration of TMZ and hence its chemotherapeutic activity [29]. Another hypothesis to explain these effects could be an increase in tumour perfusion/oxygenation ratio [28, 30, 31] which increases the efficacy of chemotherapy. Future experiments might consider the mechanisms of action that underlie this synergistic effect.

For early evaluation of treatment efficacy, multimodal imaging allows characterization of drug effects on tumour cells and the vascular system soon after the initiation of treatment when no effect on tumour volume is detectable with anatomical MRI. In line with our previous results [9], we clearly demonstrated that [<sup>18</sup>F]FLT uptake, oedema and fCBV are

correlated with treatment efficacy. However, [<sup>18</sup>F]FLT uptake provides the highest specificity and sensitivity (specificity/sensitivity 86 %/89 % for [<sup>18</sup>F]FLT, 80 %/55 % for oedema and 78 %/70 % for fCBV). Our results are in accordance with those of Schwarzenberg et al. [11] and Zhao et al. [32] who also demonstrated that [<sup>18</sup>F]FLT uptake is predictive of treatment efficacy in patients with recurrent GBM.

In the present study, we used [<sup>18</sup>F]FLT to assess response to treatment in a recurrent model of GBM. Numerous radiotracers have been proposed in the literature for estimating therapeutic efficacy in patients with recurrent or newly diagnosed glioblastoma (or in preclinical models) including tracers of proliferation such as [<sup>18</sup>F]FLT [9, 12, 16], tracers of apoptosis [33], and radiolabelled amino acids such as [<sup>11</sup>C]MET, [<sup>18</sup>F]FET and [<sup>18</sup>F]FDOPA (3,4-dihydroxy-6-[<sup>18</sup>F]fluoro-L-phenylalanine). Interestingly, in a study comparing [<sup>18</sup>F]FLT and [<sup>18</sup>F]FDOPA in the evaluation of patients with recurrent brain tumour receiving bevacizumab and irinotecan, [<sup>18</sup>F]FLT was more predictive of overall survival than [<sup>18</sup>F]FDOPA [34]. A principal advantage of

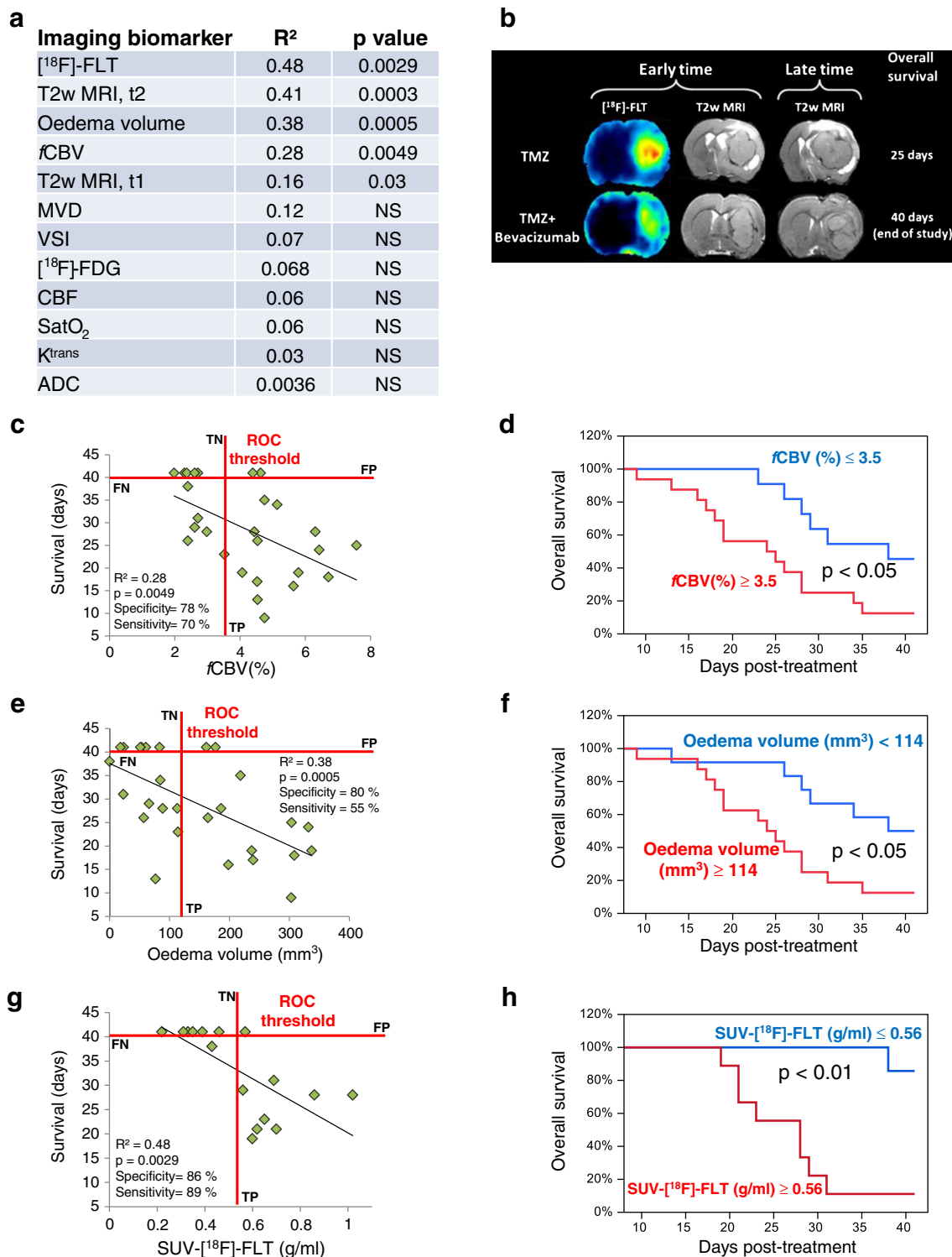


**Fig. 6** Predictive value of imaging biomarkers. **a** Correlation coefficients ( $R^2$ ) for linear regression and the corresponding  $p$  values between each of the imaging biomarkers and overall survival. **b** Imaging in two representative animals showing the value of [<sup>18</sup>F]FLT uptake in predicting treatment efficacy. **c**, **e**, **g** Correlations between fCBV (**c**),

oedema volume (**e**) and [<sup>18</sup>F]FLT uptake (**g**) and overall survival. **d**, **f**, **h** Kaplan-Meier survival curves according to cut-off values derived from the area under the ROC curves for fCBV (**d**), oedema volume (**f**) and [<sup>18</sup>F]FLT uptake (**h**). *NS* not significant, *TP* true-positive, *TN* true-negative. *FP* false-positive, *FN* false-negative

[<sup>18</sup>F]FLT compared with other radiolabelled amino acids is that this biomarker provides a marked contrast between

tumour and normal-appearing brain tissue, as already discussed in newly diagnosed glioma [35].

We opted for a static and delayed acquisition of [ $^{18}\text{F}$ ]FLT, an approach not compatible with any kinetic modelling. This choice was made since a dynamic acquisition, as well as being a realistic solution for routine clinical practice, limits repeated and prolonged examinations of the animals (MRI, [ $^{18}\text{F}$ ]FDG PET and [ $^{18}\text{F}$ ]FLT PET) and avoids the risks involved in repeated anaesthesia. Furthermore, a kinetic analysis requires sequential blood sampling which could adversely affect the general physiological status of the animals. In our study, based on static acquisition, SUV was used for analysis. Wardak et al. [34] found that the SUV approach gave predictive results although inferior to those of kinetic parameters for estimating the response to treatment in recurrent glioblastoma. In our study, [ $^{18}\text{F}$ ]FLT SUV was a robust predictor of treatment efficacy but we do acknowledge that a kinetic analysis could have improved our overall understanding.

We postulate that the decrease in [ $^{18}\text{F}$ ]FLT uptake results from a decrease in blood flow, blood volume or blood–brain barrier (BBB) permeability, all of which may affect the distribution of [ $^{18}\text{F}$ ]FLT in the tumour. Although several clinical studies have shown the importance of the integrity of the BBB in relation to [ $^{18}\text{F}$ ]FLT uptake [16, 36], these investigations were centred on a comparison between low-grade and high-grade glioma. However, it is widely accepted that the BBB is not compromised in low-grade glioma and the BBB thus impedes the passage of [ $^{18}\text{F}$ ]FLT, which is not the case in glioblastoma. In our preclinical study, the permeability of the BBB was analysed dynamically with T1 mapping and we observed that, whatever the treatment, the BBB was compromised although with some differences between groups. In this study, as previously described [9, 37], [ $^{18}\text{F}$ ]FLT uptake and Gd-DOTA enhancement were closely correlated ( $R^2=0.76$ ; [Supplementary Figure](#)) although [ $^{18}\text{F}$ ]FLT uptake yielded values slightly greater than those for Gd-DOTA enhancement. In this study, for consistency among all images and so that the analysis was independent of image segmentation, we decided to use a common ROI derived from MRI and to further focus on the effects of treatment on intensity rather than on volume.

To further explore potential relationships between [ $^{18}\text{F}$ ]FLT uptake and BBB permeability, we conducted a correlation study. At the intergroup level,  $K^{\text{trans}}$  was significantly higher in the TMZ group and, in contrast, no change was observed in the TMZ+bevacizumab group. On the other hand, [ $^{18}\text{F}$ ]FLT uptake was unchanged in the TMZ group but significantly lower in the TMZ+bevacizumab group. We then performed a correlation study in which [ $^{18}\text{F}$ ]FLT uptake was expressed as a function of  $K^{\text{trans}}$  in the tumour ROI. No correlation was observed ( $R^2=0.02$ ;  $p=0.69$ ). The marked value of [ $^{18}\text{F}$ ]FLT uptake for predicting survival (not observed for  $K^{\text{trans}}$ ) would suggest that [ $^{18}\text{F}$ ]FLT changes do indeed reflect the antineoplastic action of the treatments, as corroborated by the tight correlation observed between [ $^{18}\text{F}$ ]FLT and Ki67 immunostaining.

This study had some limitations. First, it was performed in small animals and not in a patient population. It also focused on only one glioblastoma model (U251), a model chosen based on our previous experiments showing that this model exhibits most of the salient pathophysiological characteristics described in human GBM regarding hypoxia/oxygen levels, invasion and potential key mutations such as p53 [20, 38, 39]. The low efficacy observed for bevacizumab alone might be explained by the fact that this antibody was targeted for human vascular endothelial growth factor. Another limitation of this study is that dynamic acquisition and kinetic modelling for [ $^{18}\text{F}$ ]FLT uptake were not undertaken. As discussed above, these approaches may have improved the predictive value of the tracer. A statistical limitation of this study is that although we used post-hoc tests following a significant ANOVA, each ANOVA was considered separately. The predictive value of the different biomarkers was assessed by linear correlation, with no correction for multiple comparisons, which might have decreased the likelihood of false-positive findings in this study.

## Conclusion

We demonstrated the usefulness of multimodal imaging for predicting the efficacy of a chemotherapeutic regimen combined with an antiangiogenic treatment in a recurrent GBM model. Among the different biomarkers analysed in this preclinical study, [ $^{18}\text{F}$ ]FLT appeared to be the most specific and earliest indicator for the early assessment of therapeutic efficacy in our experimental paradigm. The present investigation underscores the importance of multimodal imaging in the early assessment of tumoral response to treatment since it allows the characterization, in a narrow temporal window, of various features of a tumour including cell proliferation, oedema and various parameters of the vasculature. These results reinforce the interest in and emphasize the importance of employing state-of-the-art PET/MR systems for the therapeutic management of certain GBM patients.

## Compliance with ethical standards

**Funding** This study was funded by the Institut National contre le Cancer (INCa), Roche, the Centre National de la Recherche Scientifique (CNRS), the French Ministère de l'Enseignement Supérieur et de la Recherche (MESR) and the University of Caen-Basse Normandie (UCBN), the Conseil Régional de Basse-Normandie, the European Union-Fonds Européen de Développement Régional (FEDER), the French Agence Nationale de la Recherche (ANR-11-LABX-18-01 “Investissements d’Avenir” and ANR-2011-BSV5-004-03) and the Trans Channel Neuroscience Network (TC2N).

**Conflicts of interest** Ariel Savina and Fanny Bouquet are employed by Roche.

**Ethical approval** All applicable international, national, and/or institutional guidelines for the care and use of animals were followed. All

procedures performed in studies involving animals were in accordance with the ethical standards of the institution or practice at which the studies were conducted as detailed in the “Materials and methods” section.

## References

- Stupp R, Mason WP, van den Bent MJ, Weller M, Fisher B, Taphoorn MJ, et al. Radiotherapy plus concomitant and adjuvant temozolomide for glioblastoma. *N Engl J Med*. 2005;352:987–96.
- Desjardins A, Friedman HS. Neuro-oncology: glioblastoma – community adjusts to new standard of care. *Nat Rev Neurol*. 2012;8:244–6.
- Eftimov N, Ivanov ID, Petkov AP, Nakov E. Management of recurrent high-grade gliomas. *Cancer Ther*. 2007;5:243–52.
- Taal W, Oosterkamp HM, Walenkamp AM, Dubbink HJ, Beerepoot LV, Hanse MC, et al. Single-agent bevacizumab or lomustine versus a combination of bevacizumab plus lomustine in patients with recurrent glioblastoma (BELOB trial): a randomised controlled phase 2 trial. *Lancet Oncol*. 2014;15:943–53.
- Miletic H, Niclou SP, Johansson M, Bjerkvig R. Anti-VEGF therapies for malignant glioma: treatment effects and escape mechanisms. *Expert Opin Ther Targets*. 2009;13:455–68.
- Thompson EM, Frenkel EP, Neuwelt EA. The paradoxical effect of bevacizumab in the therapy of malignant gliomas. *Neurology*. 2011;76:87–93.
- Friedman HS, Prados MD, Wen PY, Mikkelsen T, Schiff D, Abrey LE, et al. Bevacizumab alone and in combination with irinotecan in recurrent glioblastoma. *J Clin Oncol*. 2009;27:4733–40.
- Van Linde ME, Verhoeff JJ, Richel DJ, van Furth WR, Reijneveld JC, Verheul HM, et al. Bevacizumab in combination with radiotherapy and temozolomide for patients with newly diagnosed glioblastoma multiforme. *Oncologist*. 2015;20:107–8.
- Corroyer-Dulmont A, Pérès EA, Petit E, Guillo J-S, Varoquaux N, Roussel S, et al. Detection of glioblastoma response to temozolomide combined with bevacizumab based on  $\mu$ MRI and  $\mu$ PET imaging reveals [18F]-fluoro-L-thymidine as an early and robust predictive marker for treatment efficacy. *Neuro Oncol*. 2013;15:41–56.
- Pope WB, Lai A, Mehta R, Kim HJ, Qiao J, Young JR, et al. Apparent diffusion coefficient histogram analysis stratifies progression-free survival in newly diagnosed bevacizumab-treated glioblastoma. *AJNR Am J Neuroradiol*. 2011;32:882–9.
- Schwarzenberg J, Czernin J, Cloughesy TF, Ellingson BM, Pope WB, Geist C, et al. 3'-Deoxy-3'-18F-fluorothymidine PET and MRI for early survival predictions in patients with recurrent malignant glioma treated with bevacizumab. *J Nucl Med*. 2012;53:29–36.
- Viel T, Schelhaas S, Wagner S, Wachsmuth L, Schwegmann K, Kuhlmann M, et al. Early assessment of the efficacy of temozolomide chemotherapy in experimental glioblastoma using [18F]FLT-PET imaging. *PLoS One*. 2013;8, e67911.
- Lemasson B, Christen T, Serduc R, Maisin C, Bouchet A, Le Duc G, et al. Evaluation of the relationship between MR estimates of blood oxygen saturation and hypoxia: effect of an antiangiogenic treatment on a gliosarcoma model. *Radiology*. 2012;265:743–52.
- Jordan BF, Magat J, Collier F, Ozel E, Fruytier AC, Marchand V, et al. Mapping of oxygen by imaging lipids relaxation enhancement: a potential sensitive endogenous MRI contrast to map variations in tissue oxygenation. *Magn Reson Med*. 2013;70:732–44.
- Emblem KE, Mouridsen K, Bjornerud A, Farrar CT, Jennings D, Borra RJH, et al. Vessel architectural imaging identifies cancer patient responders to anti-angiogenic therapy. *Nat Med*. 2013;19:1178–83.
- Ullrich R, Backes H, Li H, Kracht L, Miletic H, Kesper K, et al. Glioma proliferation as assessed by 3'-fluoro-3'-deoxy-L-thymidine positron emission tomography in patients with newly diagnosed high-grade glioma. *Clin Cancer Res*. 2008;14:2049–55.
- Hutterer M, Nowosielski M, Putzer D, Waitz D, Tinkhauser G, Kostroń H, et al. O-(2-18F-fluoroethyl)-L-tyrosine PET predicts failure of antiangiogenic treatment in patients with recurrent high-grade glioma. *J Nucl Med*. 2011;52:856–64.
- Derlon JM, Chapon F, Noël MH, Khouri S, Benali K, Petit-Taboué MC, et al. Non-invasive grading of oligodendrogliomas: correlation between in vivo metabolic pattern and histopathology. *Eur J Nucl Med*. 2000;27:778–87.
- Chen W, Delaloye S, Silverman DHS, Geist C, Czernin J, Sayre J, et al. Predicting treatment response of malignant gliomas to bevacizumab and irinotecan by imaging proliferation with [18F] fluorothymidine positron emission tomography: a pilot study. *J Clin Oncol*. 2007;25:4714–21.
- Corroyer-Dulmont A, Pérès EA, Petit E, Durand L, Marteau L, Toutain J, et al. Noninvasive assessment of hypoxia with 3-[18F]-fluoro-1-(2-nitro-1-imidazolyl)-2-propanol ([18F]-FMISO): a PET study in two experimental models of human glioma. *Biol Chem*. 2013;394:529–39.
- Valable S, Eddi D, Constans J-M, Guillo J-S, Bernaudin M, Roussel S, et al. MRI assessment of hemodynamic effects of angiopoietin-2 overexpression in a brain tumor model. *Neuro Oncol*. 2009;11:488–502.
- Varallyay C, Muldoon L, Gahramanov S. Dynamic MRI using iron oxide nanoparticles to assess early vascular effects of antiangiogenic versus corticosteroid treatment in a glioma model. *J Cereb Blood Flow Metab*. 2009;29:853–60.
- Valable S, Petit E, Roussel S, Marteau L, Toutain J, Divoux D, et al. Complementary information from magnetic resonance imaging and (18)F-fluoromisonidazole positron emission tomography in the assessment of the response to an antiangiogenic treatment in a rat brain tumor model. *Nucl Med Biol*. 2011;38:781–93.
- Lemasson B, Valable S, Farion R, Krainik A, Rémy C, Barbier EL. In vivo imaging of vessel diameter, size, and density: a comparative study between MRI and histology. *Magn Reson Med*. 2013;69:1–3.
- Hawkins-Daarud A, Rockne RC, Anderson AR, Swanson KR. Modeling tumor-associated edema in gliomas during anti-angiogenic therapy and its impact on imageable tumor. *Front Oncol*. 2013;3:66.
- Ellingson BM, Cloughesy TF, Lai A, Nghiemphu PL, Lalezari S, Zaw T, et al. Quantification of edema reduction using differential quantitative T2 (DQT2) relaxometry mapping in recurrent glioblastoma treated with bevacizumab. *J Neurooncol*. 2012;106:111–9.
- Roth P, Regli L, Tonder M, Weller M. Tumor-associated edema in brain cancer patients: pathogenesis and management. *Expert Rev Anticancer Ther*. 2013;13:1319–25.
- Brown JM, Wilson WR. Exploiting tumour hypoxia in cancer treatment. *Nat Rev Cancer*. 2004;4:437–47.
- Zhou Q, Gallo JM. Differential effect of sunitinib on the distribution of temozolomide in an orthotopic glioma model. *Neuro Oncol*. 2009;11:301–10.
- McGee MC, Hamner JB, Williams RF, Rosati SF, Sims TL, Ng CY, et al. Improved intratumoral oxygenation through vascular normalization increases glioma sensitivity to ionizing radiation. *Int J Radiat Oncol Biol Phys*. 2010;76:1537–45.
- Pérès EA, Gérault AN, Valable S, Roussel S. Silencing erythropoietin receptor on glioma cells reinforces efficacy of temozolomide and X-rays through senescence and mitotic catastrophe. *Oncotarget*. 2015;6:2101–19.
- Zhao F, Cui Y, Li M, Fu Z, Chen Z, Kong L, et al. Prognostic value of 3'-Deoxy-3'-18F-Fluorothymidine ([18F] FLT PET) in patients with recurrent malignant gliomas. *Nucl Med Biol*. 2014;41:710–5.



33. Oborski MJ, Laymon CM, Lieberman FS, Drappatz J, Hamilton RL, Mountz JM. First use of 18F-labeled ML-10 PET to assess apoptosis change in a newly diagnosed glioblastoma multiforme patient before and early after therapy. *Brain Behav.* 2014;4:312–5.
34. Wardak M, Schiepers C, Cloughesy TF, Dahlbom M, Phelps ME, Huang SC. 18F-FLT and 18F-FDOPA PET kinetics in recurrent brain tumors. *Eur J Nucl Med Mol Imaging.* 2014;41:1199–209.
35. Jeong SY, Lim SM. Comparison of 3'-deoxy-3'-[(18F)]fluorothymidine PET and O-(2-[(18F)]fluoroethyl)-L-tyrosine PET in patients with newly diagnosed glioma. *Nucl Med Biol.* 2012;39:977–81.
36. Seung JC, Jae SK, Jeong HK, Seung JO, Jeong GL, Chang JK, et al. [18F]3'-deoxy-3'-fluorothymidine PET for the diagnosis and grading of brain tumors. *Eur J Nucl Med Mol Imaging.* 2005;32:653–9.
37. Yamamoto Y, Wong TZ, Turkington TG, Hawk TC, Reardon DA, Coleman RE. 3'-Deoxy-3'-[F-18]fluorothymidine positron emission tomography in patients with recurrent glioblastoma multiforme: comparison with Gd-DTPA enhanced magnetic resonance imaging. *Mol Imaging Biol.* 2006;8:340–7.
38. Radaelli E, Ceruti R, Patton V, Russo M, Degraffi A, Croci V, et al. Immunohistopathological and neuroimaging characterization of murine orthotopic xenograft models of glioblastoma multiforme recapitulating the most salient features of human disease. *Histol Histopathol.* 2009;24:879–91.
39. Godoy PR, Mello SS, Magalhães DA, Donaires FS, Nicolucci P, Donadi EA, et al. Ionizing radiation-induced gene expression changes in TP53 proficient and deficient glioblastoma cell lines. *Mutat Res.* 2013;756:46–55.